ORIGINAL SCIENTIFIC PAPER

CROATICA CHEMICA ACTA

Croat. Chem. Acta **2027**, *100*(1)
Published online: November 21, 2026
DOI: 10.5562/cca4412

HKD 1926

Naphthalene Bis-carboxamide Amino Acid Bioconjugates as Super Organogelators

Zoran Kokan,[1] Tamara Miljuš,[1] Janja Makarević,[2,†] Goran Štefanić,[3] Tihomir Pospišil,[2] Leo Frkanec,[2] Berislav Perić,[1,*] Srećko I. Kirin[1,#]

[1] Ruđer Bošković Institute, Division of materials chemistry, Bijenička cesta 54, 10000 Zagreb, Croatia
[2] Ruđer Bošković Institute, Division of organic chemistry and biochemistry, Bijenička cesta 54, 10000 Zagreb, Croatia
[3] Ruđer Bošković Institute, Division of materials physics, Bijenička cesta 54, 10000 Zagreb, Croatia
* Corresponding author's e-mail address: bperic@irb.hr
# Corresponding author's e-mail address: skirin@irb.hr
† In memoriam, December 2, 2020

RECEIVED: August 14, 2026 ✶ REVISED: August 24, 2026 ✶ ACCEPTED: August 25, 2026

DEDICATED TO THE CENTENARY OF CROATICA CHEMICA ACTA (1927 – 2027)

Abstract: A series of 1,4- and 2,6-disubstituted naphthalene amides appended with glycine, alanine, phenylalanine, and hexylamine moieties were prepared and fully characterized, including five single crystal X-ray structures. Chiral amino acid derivatives acted as super gelators of non-polar organic solvents with critical gelling concentration as low as 0.014 % *w/v*. We use variable temperature NMR, FTIR, UV-Vis and CD measurements to identify hydrogen bonding and aromatic interactions as driving forces for molecular association and gelation, with TEM imaging confirming the fibrillar nature of the xerogels. Our results establish chiral naphthalene amino acid bioconjugates as highly efficient organogelators, and may serve as models for more elaborate super gelators with applications in sensing and catalysis.

Keywords: naphthalene bioconjugates, amino acids, chirality, supramolecular gels, self-association.

INTRODUCTION

CHIRALITY plays an important role in the recognition process of small molecules, albeit still not fully understood in terms of self-recognition.[1] Self-assembly phenomena is ubiquitous in both biological and artificial systems, where various chiral supramolecular associates can form through hierarchical assembly of multiple molecules,[2] governed by non-covalent interactions. Such higher order structures often exhibit supramolecular chirality in solution,[3] and under particular conditions may yield different chiral nano-structures and smart materials.[4]

Supramolecular gels[5–7] are a very robust class of smart soft materials[8] applied in different areas of academic and industrial research covering crystallization,[9] drug delivery,[10,11] electronic devices,[12] wound repair,[13] and bio-imaging,[14] just to name a few contemporary examples. They frequently arise through the assembly of small molecular weight molecules that exhibit directional interactions and aggregation, resulting in fibrillar intertwined nano structures that entrap the solvent in a solid-like state. Amino acids are frequently employed as chiral building blocks in supramolecular gels due to their natural abundance and high propensity for molecular association through hydrogen bonding. Such peptide-based supramolecular gels, which are frequently stimuli responsive,[15] may be employed in e.g. protein mimics,[16] for detecting important analytes,[17] removing environmental pollutants,[18,19] or for the recognition of chiral molecules.[20] The latter is especially interesting from the aspect of asymmetric catalysis,[21] where various supramolecular nanostructures can induce enantio-selectivity in a reaction.

In our research on supramolecular asymmetric transition metal catalysis using amino acid bioconjugated ligands,[22–24] we use model C_2-symmetric systems comprised of an aromatic core appended with amino acids

This work is licensed under a Creative Commons Attribution 4.0 International License.

to study supramolecular interactions between the molecules. Understanding these interactions is important for inducing enantioselectivity via backdoor induction[23,24] through predictive hydrogen bonding and aromatic stacking. During the course of our investigations, some of the naphthalene derivatives exhibited propensity to form gels during isolation, and we decided to further investigate these properties in more detail. This is perhaps not surprising since various compounds disubstituted with amino acids exhibit supramolecular polymerization and gelation, such as oxalamide[25–27] and naphthalene bis-imide[28–30] systems. Herein we report a series of naphthalene bis-carboxamide amino acid bioconjugates that exhibit super organogelation, expanding on the C_2-symmetric chiral supramolecular gelators.[31]

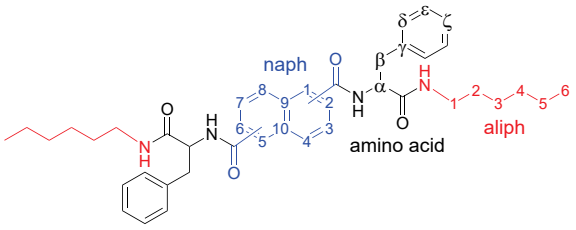
EXPERIMENTAL

General Remarks

Reactions were carried out in ordinary glassware and chemicals were used as purchased from commercial suppliers without further purification. Pure L-amino acids were used. Reactions were monitored by TLC on Silica Gel 60 F254 plates and detected with UV lamp (254 nm) or iodine; compounds were purified using column chromatography on silica. Mass spectra were measured on a HPLC-MS system, coupled with 6410 Triple-Quadrupole mass spectrometer, operating in a positive ESI mode. High resolution mass spectra were obtained on a MALDI TOF-TOF instrument using CHCA matrix. NMR spectra were obtained on spectrometers operating at 300.13 or 600.13 MHz for ^{1}H and 75.47 or 150.92 MHz for ^{13}C nuclei. Chemical shifts, δ (ppm), indicate a downfield shift from the internal standard, tetramethylsilane, TMS, for ^{1}H NMR or residual solvent signal for ^{13}C NMR (39.52 ppm DMSO-d_6).

Critical gelling concentration (CGC), reflecting gelation efficiency, was determined as following. Solvent was added via a syringe to the weighed compound in a septum-capped test tube (1.1 cm diameter) and heated to boiling until the compound dissolved, followed by slow cooling in a water bath (20 ± 3 °C). If no flow was observed upon inverting the test tube, more solvent was added until the test tube showed noticeable flow. The last gel formation (i.e. no flow observed after 1 up to 10 days) determines the CGC, expressed as % *w*/*v*.

FTIR investigations were performed on an ABB Bomen MB 102 FTIR-spectrometer in the sealed cells (Specac, path length 0.05 mm or 0.025 nm, CaF_2 windows). Temperature dependent UV measurements were recorded on a Varian Cary 100 Bio spectrophotometer and CD spectra on a JASCO J815 spectrophotometer in the QS Hellma cells with detachable windows (light path 0.1 mm) and absorption cells (light path 1 mm). The transmission



Scheme 1. Numbering scheme for ^{13}C NMR spectra, on the Phe derivative example.

electron micrographs were taken on an EM 10 A Zeiss or FEI Morgagni 268D transmission electron microscope. A small amount of the gel sample was placed on a carbon-coated copper grid (100 mesh). The sample were coated with Pd or negatively stained with PWK (dipotassium phosphotungstate).

The X-ray intensity data for **1**, **2m**, **2o**, **4b**, and **5** were collected on Xcalibur, Ruby, Nova CCD diffractometer using monochromatic Cu-*Kα* (λ = 1.54184 Å) radiation at room temperature. Basic experimental data are given in Supplementary material. The data were processed with the *CrysAlis* Pro program[32] used for unit cell determination and data reduction. Structures were solved by direct methods using the SHELXT program[33] and refined against F^2 on all data by the SHELXL program.[34] All non-hydrogen atoms were refined in an anisotropic model of atomic displacement parameters (ADPs). For structure **2m** refinement with possible 2- fold twinning law was used. Although twinning refinement revealed negligible volume fraction of second component, the overall set of data contained no significant outlier reflections [with $(I_{obs}-I_{calc})/\sigma > 10$]. If such reflections appeared during other refinements (for example, 2 reflections for **2o**) they were excluded from the data set. Large atomic displacement parameters (ADPs) for atoms in aliphatic chains of **4b** show strong disorder, also supported by the highest peaks in the different electron density found their vicinity. For this reason, in the refinement of **4b**, rigid body restraints (RIGU) and restraint of mutually identical distances and angles in two aliphatic chains were used (SAME). Positions of hydrogen atoms were treated mixed, i.e. parameters for hydrogen atoms in N–H groups were completely refined, while hydrogen atoms attached to carbon atoms were refined in the riding model, i.e. they were calculated according to the positions of the carbon atoms. C–H distances for aromatic, methylene and methyl H-atoms were constrained to 0.93, 0.97 and 0.96 Å, respectively, with isotropic ADP parameter U_{iso}(H) = 1.2 × U_{iso}(C) for aromatic and methylene H-atoms and U_{iso}(H) = 1.5 × U_{iso}(C) for methyl H-atoms. Torsion angles of the methyl groups were refined (AFIX 137), except for the terminal atoms in aliphatic chains od **4b**, where tighter constraint for riding

model of methyl group was used (AFIX 33). The CCDC 2580557–2580561 contain the supplementary crystallographic data for this paper.

Synthesis

Boc-Aa-NH-*n*C_6H_{13}, General Procedure

Boc-protected amino acid (1 eq.) and *N*,*N*'-dicyclohexylcarbodiimide (1 eq.) were dissolved in DCM (50 cm^3). After the reaction mixture was stirred at room temperature for 1 h, hexylamine (1.5 eq.) was added and continued stirring for 24 h. Then, the reaction mixture was filtered (white band) and purified by column chromatography (ethyl acetate – hexane gradient, depending on a particular case).

Synthesis of Boc-Gly-*n*C_6H_{13}

Boc-Gly-OH (1.314 g, 7.5 mmol), DCC (1.547 g, 7.5 mmol) and hexylamine (1.5 cm^3, 11.25 mmol). Yield: 989.6 mg (3.8 mmol, 51.1 %). M_r ($C_{13}H_{26}N_2O_3$) = 258.36, ESI-MS (*m*/*z*): 281 [5 %, M + Na^+], 259 [16 %, M + H^+], 225 [5 %, M–*t*-butyl + Na^+], 203 [38 %, M–*t*-butyl + H^+], 159 [100 %, Boc-Gly + H^+], 102 [8 %, hexylamine + H^+]. ^{1}H NMR (300 MHz, DMSO-d_6) δ/ppm: 7.65 (t, 1H, *J* = 5 Hz), 6.84 (t, 1H, *J* = 5.5 Hz), 3.48 (d, 2H, *J* = 6 Hz), 3.04 (q, 2H, J_1 = 6 Hz, J_2 = 6.5 Hz), 1.24–1.38 (m, 17H), 0.86 (t, 3H, *J* = 7 Hz).

Synthesis of Boc-Ala-*n*C_6H_{13}

Boc-Ala-OH (946 mg, 5 mmol), DCC (1.032 g, 5 mmol) and hexylamine (1 cm^3, 7.61 mmol). Yield: 764 mg (2.8 mmol, 56.1 %). M_r ($C_{14}H_{28}N_2O_3$) = 272.38, ESI-MS (*m*/*z*): 295 (100%, [M + Na^+]). ^{1}H NMR (300 MHz, DMSO-d_6) δ/ppm: 7.67 (t, 1H, *J* = 5 Hz), 6.79 (d, 1H, *J* = 7.5 Hz), 3.84–3.94 (m, 1H), 2.93–3.11 (m, 2H), 1.12–1.37 (m, 20H), 0.85 (t, 3H, *J* = 7 Hz).

Synthesis of Boc-Phe-*n*C_6H_{13}

Boc-Phe-OH (1.331 g, 5.02 mmol), DCC (1.072 g, 5.19 mmol) and hexylamine (1 cm^3, 7.61 mmol). Yield: 1 g (2.87 mmol, 57.4 %). M_r ($C_{20}H_{32}N_2O_3$) = 348.48, ESI-MS (*m*/*z*): 349 (30 %, [M + H^+]). ^{1}H NMR (300 MHz, DMSO-d_6) δ/ppm: 7.80 (t, 1H, *J* = 5.5 Hz), 7.17–7.28 (m, 5H), 6.84 (d, 1H, *J* = 8.5 Hz), 4.06–4.14 (m, 1H), 2.69–3.09 (m, 4H), 1.23–1.30 (m, 17H), 0.86 (t, 3H, *J* = 7 Hz).

Boc Protecting Group Removal

Boc-Aa-NH-*n*C_6H_{13} was dissolved in DCM (5 cm^3) and trifluoroacetic acid was added (5 cm^3). The reaction mixture was stirred at room temperature for 2 h, then evaporated *in vacuo* (rotavap) and neutralized with DIPEA (1 cm^3). The crude product was used in further synthesis without purification.

General Synthetic Procedure for Naphthalene Derivatives

Naphthalene dicarboxylic acid was dissolved in DCM (50 cm^3) in a round bottom flask wrapped with aluminum foil, and TBTU (2 eq.), HOBt × H_2O (2 eq.) and DIPEA (8 eq.) were added and stirred for 1 h at room temperature. Then the amino acid or amine (2.5 eq., *N*-unprotected) were added and continued stirring for 24–48 h. After that, the reaction mixture was extracted with $NaHCO_3$ (3 × 50 cm^3, sat.) and subjected to chromatography on silica (DCM: methanol).

Synthesis of 1

2,6-Naphthalene dicarboxylic acid (216.19 mg, 1 mmol), TBTU (642.6 mg, 2 mmol), HOBt × H_2O (270.3 mg, 2 mmol), H-Gly-OMe·× HCl (314.9 mg, 2.5 mmol), DIPEA (1.4 cm^3, 8 mmol), reaction time: 48 h. The reaction mixture was cloudy (slightly gelating) and was therefore subjected to column chromatography (40 g silica, eluent 1 % → 5 % methanol in DCM) without washing. The fractions containing the product were evaporated *in vacuo*, washed with DCM (5 × 5 cm^3), centrifuged, decanted and the solid was dried *in vacuo* (10^{-2} mbar). Yield: 209.4 mg (54.7 %). ESI-MS (*m*/*z*): 359 (100 %, [M + $H]^+$). MALDI-HRMS (*m*/*z*): calcd. 359.1237 ($C_{18}H_{18}N_2O_6$ + H^+), found: 359.1227. ^{1}H NMR (300.13 MHz, DMSO-d_6) δ/ppm: 3.68 (s, 6H), 4.09 (d, 4H, *J* = 6 Hz), 8.01 (dd, 2H, J_1 = 8.5 Hz, J_2 = 1.5 Hz), 8.14 (d, 2H, *J* = 8.5 Hz), 8.54 (s, 2H), 9.18 (t, 2H, *J* = 6 Hz). ^{13}C NMR (150.92 MHz, DMSO-d_6) δ/ppm: 41.3 (α), 51.7 (OMe), 124.8 (C3, C7), 127.4 (C1, C5), 129.2 (C4, C8), 132.6 (C9, C10), 133.4 (C2, C6), 166.5 (CO^{Naph}), 170.3 (CO^{Gly}).

Synthesis of 2

1,4-Naphthalene dicarboxylic acid (162.2 mg, 0.75 mmol), TBTU (482.7 mg, 1.5 mmol), HOBt × H_2O (202.7 mg, 1.5 mmol), DIPEA (1 cm^3, 6 mmol), H-Gly-OMe·× HCl (235.4 mg, 1.88 mmol), reaction time: 72 h. The mixture was washed with saturated $NaHCO_3$ (3 × 50 cm^3), dried on Na_2SO_4 and subjected to column chromatography (40 g SiO_2, eluent 1 % → 5 % methanol in DCM). Yield: 80.6 mg (27.8 %). ESI-MS (*m*/*z*): 359 (46 %, [M + $H]^+$). MALDI-HRMS (*m*/*z*): calcd. 381.1057 ($C_{18}H_{18}N_2O_6$ + Na^+), found 381.1060. ^{1}H NMR (300.13 MHz, DMSO-d_6) δ/ppm: 3.73 (s, 6H), 4.10 (d, 4H, *J* = 6 Hz), 7.59–7.66 (m, 4H), 8.27–8.34 (m, 2H), 9.03 (t, 2H, *J* = 6 Hz). ^{13}C NMR (150.92 MHz, DMSO-d_6) δ/ppm: 40.1 (α), 51.8 (OMe), 124.0 (C5, C8), 125.7 (C9, C10), 126.9 (C2, C3), 129.8 (C6, C7), 136.0 (C1, C4), 168.8 (CO^{Naph}), 170.3 (CO^{Gly}).

Synthesis of 3a

2,6-Naphthalene dicarboxylic acid (108.1 mg, 0.5 mmol), TBTU (321.7 mg, 1 mmol), HOBt × H_2O (135.2 mg, 1 mmol), Boc-Gly-NHC_6H_{13} (322.9 mg, 1.25 mmol) and DIPEA (0.69 cm^3, 4 mmol), reaction time: 24 h. The mixture slightly gelated and stirring was turned off. After 20 min. the mixture separated into upper gelated and lower clear and yellowish level. It was separated in the separation funnel and dried under vacuum. Resulting compound was washed with MeOH (3 × 10 cm^3), centrifuged, decanted and dried

on rotovapor. Yield: 194.9 mg (78.5 %). ESI-MS (*m*/*z*): 519 (100 %, $[M + Na]^+$), 497 (98 %, $[M + H]^+$). MALDI-HRMS (*m*/*z*): calcd. 497.3122 ($C_{28}H_{40}N_4O_4 + H^+$), found 497.3098. ^{1}H NMR (300.13 MHz, DMSO-d_6) δ/ppm: 0.81–0.91 (m, 6H), 1.19–148 (m, 16H), 3.08 (q, 4H, J_1 = 6 Hz, J_2 = 6.5 Hz), 3.90 (d, 4H, J = 6 Hz), 7.89 (t, 2H, J = 5.5 Hz), 8.02 (dd, 2H, J_1 = 8.5 Hz, J_2 = 1 Hz), 8.11 (d, 2H, J = 8.5 Hz), 8.54 (s, 2H), 8.89 (t, 2H, J = 6 Hz). ^{13}C NMR (150.92 MHz, DMSO-d_6) δ/ppm: 13.9 ($C6^{Aliph}$), 22.0 ($C5^{Aliph}$), 26.0 ($C3^{Aliph}$), 29.1 ($C2^{Aliph}$), 31.0 ($C4^{Aliph}$), 38.6 ($C1^{Aliph}$), 42.8 (α), 125.0 (C3, C7), 127.4 (C1, C5), 128.9 (C4, C8), 132.9 (C9, C10), 133.4 (C2, C6), 166.3 (CO^{Naph}), 168.6 (CO^{Gly}).

Synthesis of 3b

2,6-Naphtalene dicarboxylic acid (127.9 mg, 0.6 mmol), TBTU (386.2 mg, 1.2 mmol), HOBt × H_2O (162.2 mg, 1.2 mmol), Boc-Ala-NHC_6H_{13} (403.6 mg, 1.48 mmol) and DIPEA (0.85cm^3, 4.8 mmol), reaction time: 96 h. The reaction mixture was cloudy (slightly gelating) and was therefore subjected to column chromatography (40 g silica, eluent 3 % → 5 % methanol in DCM) without washing. The fractions containing the product were evaporated *in vacuo*, washed with DCM (3 × 5 cm^3), centrifuged, decanted and the solid was dried *in vacuo* (10^{-2} mbar). Yield 245.8 mg (78.1 %). ESI-MS (*m*/*z*): 525 (78 %, $[M + H]^+$). MALDI-HRMS (*m*/*z*): calcd. 547.3254 ($C_{30}H_{44}N_4O_4 + Na^+$), found 547.3269. ^{1}H NMR (600.14 MHz, DMSO-d_6) δ/ppm: 0.82–0.87 (m, 6H), 1.22–1.29 (m, 12H), 1.34–1.47 (m, 10H), 3.02–3.12 (m, 4H), 4.46–4.53 (m, 2H), 7.90 (t, 2H, J = 5.5 Hz), 8.02 (d, 2H, J = 8.5 Hz), 8.09 (d, 2H, J = 8.5 Hz), 8.55 (s, 2H), 8.65 (d, 2H, J = 7.5 Hz). ^{13}C NMR (150.92 MHz, DMSO-d_6) δ/ppm: 13.8 ($C6^{Aliph}$), 18.1 (β), 22.0 ($C5^{Aliph}$), 25.9 ($C3^{Aliph}$), 29.0 ($C2^{Aliph}$), 30.9 ($C4^{Aliph}$), 38.5 ($C1^{Aliph}$), 49.1 (α), 125.1 (C3, C7), 127.4 (C1, C5), 128.7 (C4, C8), 132.9 (C9, C10), 133.2 (C2, C6), 165.8 (CO^{Naph}), 172.0 (CO^{Ala}).

Synthesis of 3c

2,6-Naphtalene dicarboxylic acid (116.2 mg, 0.52 mmol), TBTU (334.7 mg, 1.04 mmol), HOBt × H_2O (140.5 mg, 1.04 mmol), Boc-Phe-NHC_6H_{13} (453 mg, 1.3 mmol) and DIPEA (0.73 cm^3, 4.16 mmol), reaction time: 72 h. The reaction mixture gelated and was filtered through G3 filter crucible and washed with MeOH (3 × 3 cm^3). Resulting precipitate was transferred into a flask with 5 cm^3 MeOH and dried *in vacuo* (10^{-2} mbar). Yield: 225.8 mg, 64.2 %. ESI-MS (*m*/*z*): 699 (24 %, $[M + Na]^+$), 677 (23 %, $[M + H]^+$). MALDI-HRMS (*m*/*z*): calcd. 677.4061 ($C_{42}H_{52}N_4O_4 + H^+$), found 677.4082. ^{1}H NMR (300.13 MHz, DMSO-d_6) δ/ppm: 0.80–0.89 (m, 6H), 1.17–1.45 (m, 16H), 2.97–3.17 (m, 8H), 4.67–4.78 (m, 2H), 7.12–7.19 (m, 2H), 7.22–7.29 (m, 4H), 7.32–7.38 (m, 4H), 7.92 (dd, 2H, J_1 = 8.5 Hz, J_2 = 1 Hz), 8.00–8.07 (m, 4H), 8.43 (s, 2H), 8.73 (d, 2H, J = 8.5 Hz). ^{13}C NMR (150.92 MHz, DMSO-d_6) δ/ppm: 13.8 ($C6^{Aliph}$), 22.0 ($C5^{Aliph}$), 25.9 ($C3^{Aliph}$), 28.9 ($C2^{Aliph}$), 30.9 ($C4^{Aliph}$), 37.5 (β), 38.5 ($C1^{Aliph}$), 55.0 (α), 125.0 (C3, C7), 126.2 (ζ), 127.3 (C1, C5), 128.0 (δ), 128.7 (C4, C8), 129.1 (ε), 132.9 (C9, C10), 133.2 (C2, C6), 138.3 (γ), 165.9 (CO^{Naph}), 170.8 (CO^{Phe}).

Synthesis of 4a

1,4-Naphtalene dicarboxylic acid (108.1 mg, 0.5 mmol), TBTU (321.7 mg, 1 mmol), HOBt × H_2O (135.2 mg, 1 mmol), Boc-Gly-NHC_6H_{13} (322.9 mg, 1.25 mmol) and DIPEA (0.69 cm^3, 4 mmol), reaction time: 48 h. The reaction mixture was washed with $NaHCO_3$ (50 cm^3, sat.) and H_2O (50 cm^3), and dried on Na_2SO_4. The crude product was purified by column chromatography (40 g SiO_2, eluent 1 % → 5 % methanol in DCM). Yield: 91.2 mg (36.7 %). ESI-MS (*m*/*z*): 519 (30 %, $[M + Na]^+$), 497 (100 %, $[M + H]^+$). MALDI-HRMS (*m*/*z*): calcd. 519.2541 ($C_{28}H_{40}N_4O_4 + Na^+$), found 519.2516. ^{1}H NMR (600.14 MHz, DMSO-d_6) δ/ppm: 0.83–0.91 (m, 6H), 1.22–1.34 (m, 12H), 1.40–1.47 (m, 4H), 3.12 (q, 4H, J_1 = 6 Hz, J_2 = 7 Hz), 3.92 (d, 4H, J = 6 Hz), 7.57–7.61 (m, 2H), 7.66 (s, 2H), 7.92 (t, 2H, J = 5.5 Hz), 8.33–8.37 (m, 2H), 8.72 (t, 2H, 6 Hz). ^{13}C NMR (150.92 MHz, DMSO-d_6) δ/ppm: 13.9 ($C6^{Aliph}$), 22.0 ($C5^{Aliph}$), 26.0 ($C3^{Aliph}$), 29.1 ($C2^{Aliph}$), 31.0 ($C4^{Aliph}$), 38.6 ($C1^{Aliph}$), 42.4 (α), 124.1 (C5, C8), 125.9 (C9, C10), 126.7 (C2, C3), 129.9 (C6, C7), 136.2 (C1, C4), 168.4 (CO^{Naph}), 168.5 (CO^{Gly}).

Synthesis of 4b

1,4-Naphtalene dicarboxylic acid (108.1 mg, 0.5 mmol), TBTU (321.7 mg, 1 mmol), HOBt × H_2O (135.2 mg, 1 mmol), Boc-Ala-NHC_6H_{13} (340.3 mg, 1.25 mmol) and DIPEA (0.7 cm^3, 4 mmol); reaction time: 48 h. The reaction mixture was washed with $NaHCO_3$ (50 cm^3, sat.) and H_2O (50 cm^3), and dried on Na_2SO_4. The crude product was separated by column chromatography (40 g SiO_2, eluent 1 % → 5 % methanol in DCM). Yield: 103.1 mg (39.2 %). ESI-MS (*m*/*z*): 525 (100 %, $[M + H]^+$). MALDI-HRMS (*m*/*z*): calcd. 525.3435 ($C_{30}H_{44}N_4O_4 + H^+$), found 525.3416. ^{1}H NMR (300.13 MHz, DMSO-d_6) δ/ppm: 0.82–0.91 (m, 6H), 1.22–1.37 (m, 18H), 1.39–1.50 (m, 4H), 3.02–3.22 (m, 4H), 4.46–4.56 (m, 2H), 7.54–7.6 (m, 2H), 7.62 (s, 2H), 7.91 (t, 2H, J = 5.5 Hz), 8.23–8.29 (m, 2H), 8.62 (d, 2H, J = 7.5 Hz). ^{13}C NMR (150.92 MHz, DMSO-d_6) δ/ppm: 13.4 ($C6^{Aliph}$), 18.0 (β), 22.0 ($C5^{Aliph}$), 25.9 ($C3^{Aliph}$), 29.0 ($C2^{Aliph}$), 30.9 ($C4^{Aliph}$), 38.5 ($C1^{Aliph}$), 48.9 (α), 124.1 (C5, C8), 125.8 (C9, C10), 126.6 (C2, C3), 129.9 (C6, C7), 136.1 (C1, C4), 167.9 (CO^{Naph}), 172.0 (CO^{Ala}).

Synthesis of 4c

1,4-Naphtalene dicarboxylic acid (105.9 mg, 0.49 mmol), TBTU (315.4mg, 0.98 mmol), HOBt × H_2O (105.9mg, 0.98 mmol), Boc-Ala-NHC_6H_{13} (340.3 mg, 1.23 mmol) and DIPEA (0.7 cm^3, 4 mmol); reaction time: 48 h. The reaction mixture slightly gelated and was therefore subjected to column chromatography (40 g silica, eluent 2 % methanol in DCM) without washing. Yield: 136.1 mg (41.1 %). ESI-MS (*m*/*z*): 677 (100 %, $[M + H]^+$). MALDI-HRMS (*m*/*z*): calcd.

699.3879 ($C_{42}H_{52}N_4O_4$ + Na^+), found 699.3906. ^{1}H NMR (300.13 MHz, DMSO-d_6) δ/ppm: 0.82–0.92 (m, 6H), 1.21–1.49 (m, 16H), 2.89 (dd, 2H, J_1 = 13.5 Hz, J_2 = 10.5 Hz), 3.04–3.2 (m, 6H), 4.74–4.87 (m, 2H), 7.19–7.45 (m, 14H), 7.68–7.76 (m, 2H), 8.04 (t, 2H, J = 5.5 Hz), 8.68 (d, 2H, J = 8.5 Hz). ^{13}C NMR (150.92 MHz, DMSO-d_6) δ/ppm: 13.3 (C6^{Aliph}), 21.6 (C5^{Aliph}), 25.6 (C3^{Aliph}), 28.6 (C2^{Aliph}), 30.6 (C4^{Aliph}), 37.3 (β), 38.4 (C1^{Aliph}), 54.3 (α), 123.4 (C5, C8), 125.2 (ζ), 125.9 (C9, C10), 126.0 (C2, C3), 127.6 (δ), 128.9 (ε), 129.4 (C6, C7), 135.9 (C1, C4), 137.8 (γ), 167.5 (CO^{Naph}), 170.3 (CO^{Phe}).

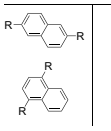
Synthesis of 5

2,6-Naphtalene dicarboxylic acid (216.19 mg, 1 mmol), TBTU (642.6 mg, 2 mmol), HOBt × H_2O (270.3 mg, 2 mmol), hexylamine (0.33 cm^3, 2.5 mmol) and DIPEA (1.4 cm^3, 8 mmol); reaction time 98 h. The reaction mixture slightly gelated and was therefore subjected to column chromatography (40 g silica, eluent 1 % methanol in DCM) without washing. Yield: 97.5 mg (25.2 %). ESI-MS (*m*/*z*): 383 (100 %, [M + H]$^+$). MALDI-HRMS (*m*/*z*): calcd. 383.2693 ($C_{24}H_{34}N_2O_2$ + H^+), found 383.2686. ^{1}H NMR (600.14 MHz, DMSO-d_6) δ/ppm: 0.83–0.92 (m, 6H), 1.26–1.38 (m, 12H), 1.51–1.60 (m, 4H), 3.26 3.35 (m, 2H, water peak overlap), 7.91–8.12 (m, 4H), 8.41–8.48 (m, 2H), 8.59–8.67 (m, 2H). ^{13}C NMR (150.92 MHz, DMSO-d_6) δ/ppm: 13.7 (C6^{Aliph}), 21.9 (C5^{Aliph}), 26.1 (C3^{Aliph}), 29.0 (C2^{Aliph}), 30.9 (C4^{Aliph}), 39 (C1^{Aliph}, solvent peak overlap), 124.8 (C3, C7), 126.8 (C1, C5), 128.7 (C4, C8), 133.1 (C9, C10), 133.4 (C2, C6), 165.9 (CO^{Naph}).

Synthesis of 6

1,4-Naphtalene dicarboxylic acid (216.19 mg, 1 mmol), TBTU (642.6 mg, 2 mmol), HOBt × H_2O (270.3 mg, 2 mmol), hexylamine (0.33 cm^3, 2.5 mmol) and DIPEA (1.4 cm^3, 8 mmol); reaction time: 72 h. The reaction mixture was washed with saturated $NaHCO_3$ (100 cm^3) and H_2O (100 cm^3), and dried on Na_2SO_4. The crude product was purified by column chromatography (40 g SiO_2, eluent 1 % → 5 % methanol in DCM). Yield: 154.8 mg (40.5 %). ESI-MS (*m*/*z*): 383 (100 %, [M + H]$^+$). MALDI-HRMS (*m*/*z*): calcd. 383.2693 ($C_{24}H_{34}N_2O_2$ + H^+), found 383.2679. ^{1}H NMR (300.13 MHz, DMSO-d_6) δ/ppm: 0.85–0.94 (m, 6H), 1.26–1.44 (m, 12H), 1.51–1.64 (m, 4H), 3.27–3.38 (m, 4H, solvent peak overlap), 7.52–7.64 (m, 4H), 8.13–8.21 (m, 2H), 8.51 (t, 2H, J = 5.5 Hz). ^{13}C NMR (150.92 MHz, DMSO-d_6) δ/ppm: 13.8 (C6^{Aliph}), 22.0 (C5^{Aliph}), 26.1 (C3^{Aliph}), 29.0 (C2^{Aliph}), 30.9 (C4^{Aliph}), 39.0 (C1^{Aliph}), 123.8 (C5, C8), 125.9 (C9, C10), 126.6 (C2, C3), 129.8 (C6, C7), 136.6 (C1, C4), 168.0 (CO^{Naph}).

Table 1. Designated title compounds prepared herein.

	R =				
	1	3a	3b	3c	5
	2	4a	4b	4c	6

RESULTS AND DISCUSSION

Synthesis

Compounds 1–6 (Table 1) were prepared starting from the corresponding commercially available naphthalene 2,6- or 1,4-dicarboxylic acid and *N*-deprotected amino acids or

Table 2. Critical gelling concentration for various solvents expressed as % *w*/*v* (and concentration in mM) of the gelator, indicating super gelation at room temperature.

	3b	3c	4a	4b	4c	6
H_2O	ins.	ins.	ins.	ins.	ins.	ins.
DMSO/H_2O	-	cr.	cr.	0.352 (6.7)	0.211 (3.1)	cr.
EtOH	cr.	ins.	cr.	cr.	1.54 (22.7)	cr.
(±)2-octanol	cr.	cr.	cr.	3.33 (63.5)	0.83 (12.3)	cr.
THF	cr.	ins.	cr.	2.63 (50.2)	cr.	cr.
CH_3CN	cr.	ins.	cr.	1.00 (19.1)	cr.	cr.
CH_2Cl_2	0.294 (5.6)	ins.	cr.	0.571 (10.9)	cr.	cr.
toluene	0.054 (1.0)	ins.	0.071 (1.4)	0.024 (0.45)	0.308 (4.6)	0.505 (13.2)*
o-xylene	0.037 (0.7)	ins.	0.093 (1.9)	0.026 (0.50)	0.238 (3.5)	0.680 (17.8)
m-xylene	0.060 (0.8)	ins.	0.154 (2.8)	0.025 (0.55)	0.117 (1.9)	cr.
p-xylene	0.042 (1.1)	ins.	0.139 (3.1)	0.029 (0.47)	0.127 (1.7)	cr.
decalin	0.031 (0.6)	ins.	0.075 (1.5)	0.014 (0.27)	0.073 (1.1)	0.333 (8.7)
tetralin	cr.	1.35 (20.0)	solution	solution	2.70 (40.0)	solution

ins. – insoluble or poorly soluble; cr. – crystallisation/precipitation; *gelation initiated by ultrasound.

amines, using standard peptide coupling conditions in solution. The isolation and purification of the synthesized compounds was in some cases impeded by precipitation/gelation. For the purification of several derivatives extraction or column chromatography could not be used (see Experimental section). Basic characterization of bioconjugates 1–6 was performed by ^{1}H and ^{13}C NMR spectroscopy in DMSO-d_6 as well as ESI MS and HR MALDI TOF spectrometry.

Modular compounds incorporate central aromatic moiety that allows intermolecular π-π interactions, and two side chains containing one or two amide groups per chain, that are capable of intermolecular hydrogen bonding. A series of simple amino acid moieties were chosen, namely, glycine methyl ester (**1**, **2**), *n*-hexylamides of amino acids glycine (**3a**, **4a**), alanine (**3b**, **4b**), and phenylalanine (**3c**, **4c**). Simple hexylamine derivatives (**5**, **6**) were prepared for comparison.

Gelation Studies

Gelation abilities of compounds **1**–**6** were tested in water and in a series of organic solvents of different polarity. Due to insufficient solubility of the compounds in water, binary solvent mixture water/DMSO was used. Most of the tested compounds were shown to be super gelators of organic solvents (Table 2). Compounds **1**, **2**, **3a** and **5** did not form gels with any of the investigated solvents, albeit partial formation of unstable gels was indicated for **5**. Gelation of aromatic solvents and decalin by both Ala regioisomers **3b** and **4b** is very impressive, with critical gelling concentration (CGC) well below 0.1 % *w*/*v*, comparable to the structurally similar terephtaloyl amino acid gelators.[35] Gels of **4c** are stable during the course of all the investigations. The acetonitrile gel of **4b** is prone to crystallization, with about a third of gel degraded within 24 h at room temperature. The gelation propensity of glycine derivative **4a** is comparable to that of phenylalanine derivative **4c**. All of the above results indicate substantial influence of substituents at alpha carbon of amino acids, likely effecting the ability to form stable intramolecular hydrogen bonds. Interestingly, alanine derivatives (**3b** and **4b**) showed overall better gelation properties, also found for other alanine-derived gels with different aromatic spacers.[36]

Transmission Electron Microscopy

Morphology of the xerogels was investigated by transmission electron microscopy (TEM) at twice the CGC concentration (Figure 1). Decalin xerogels exhibited different network morphologies in particular cases. For chiral compounds, fibre bundles were evident, while achiral **4a** exhibited mostly ribbon-like morphology. Both morphologies were also found in terephtalamide amino acid derived gels.[15] **4b**, as the most efficient decalin organogelator, exhibits a very compact and dense network made of fibre bundles, with minimal single fibre diameter of about 10 nm. Slightly less compact network was evident for **3b**. **4c** exhibits fibre bundles of larger and smaller diameters. They are easily broken during sample application on the copper grids for TEM. These individual fibres have a diameter of about 15–25 nm, but bigger bundles can reach up to 400 nm in diameter. This network organisation for **4c** is a few times less efficient than for **4b**. The xerogel networks of achiral organogelators consist of large aggregates. In case of glycine derivative **6c**, the network consists mostly of ribbons with very diverse diameters, and small quantity of fibre bundles.

Expectedly, solvent influence on the morphology of **4c** xerogel networks is significant. Thin and short fibres of **4c** ethanol xerogel forming spherulites do not enable efficient fibre cross-linking, resulting in poor gelation, as observed experimentally. It is interesting that this morphology is less efficient for gelation than the tape and fibre network of **4c** toluene xerogel. In general, it is expected that very fine fibrous structures result in more efficient gelation.

Spectroscopic Investigations

To obtain more information about non-covalent interactions responsible for gel formation, FTIR, UV-Vis, and CD spectroscopic investigations were performed with focus on **4b** having the best gelation properties.

Characteristic vibration bands in the FTIR spectra were investigated to elucidate self-assembly processes in the gel and pre-gelation states. **4b** dichloromethane gel exhibits very slow sol-gel transition at 16 mM concentration which enabled the real-time study of interactions during the 40 minutes span of sol to gel transformation (Figure 2). The spectra exhibit two poorly resolved N–H bands at 3432 and 3408 cm^{-1} which shift with time to 3286 and 3258 cm^{-1}, respectively. These bands likely correspond to two kinds of amide N–H (i.e. aromatic and aliphatic) within the molecule. The spectra indicated that even in the dissolved state, substantial portion of amide protons are involved in hydrogen bonding. Band of amide I at 1678 cm^{-1} reduces in intensity during the course of gelation, while two amide II bands at 1500 and 1517 cm^{-1} shift to 1550 and 1532 cm^{-1}, indicating that both C=O and N–H are involved in hydrogen bonding. This is in line with the FTIR analysis of terephthalamide derivatives in the literature.[35,37]

For **4b** decalin gel, the characteristic N–H stretching at 3272 cm^{-1} and amide I and amide II bands at 1628 cm^{-1} and 1544 cm^{-1}, respectively, also indicated hydrogen

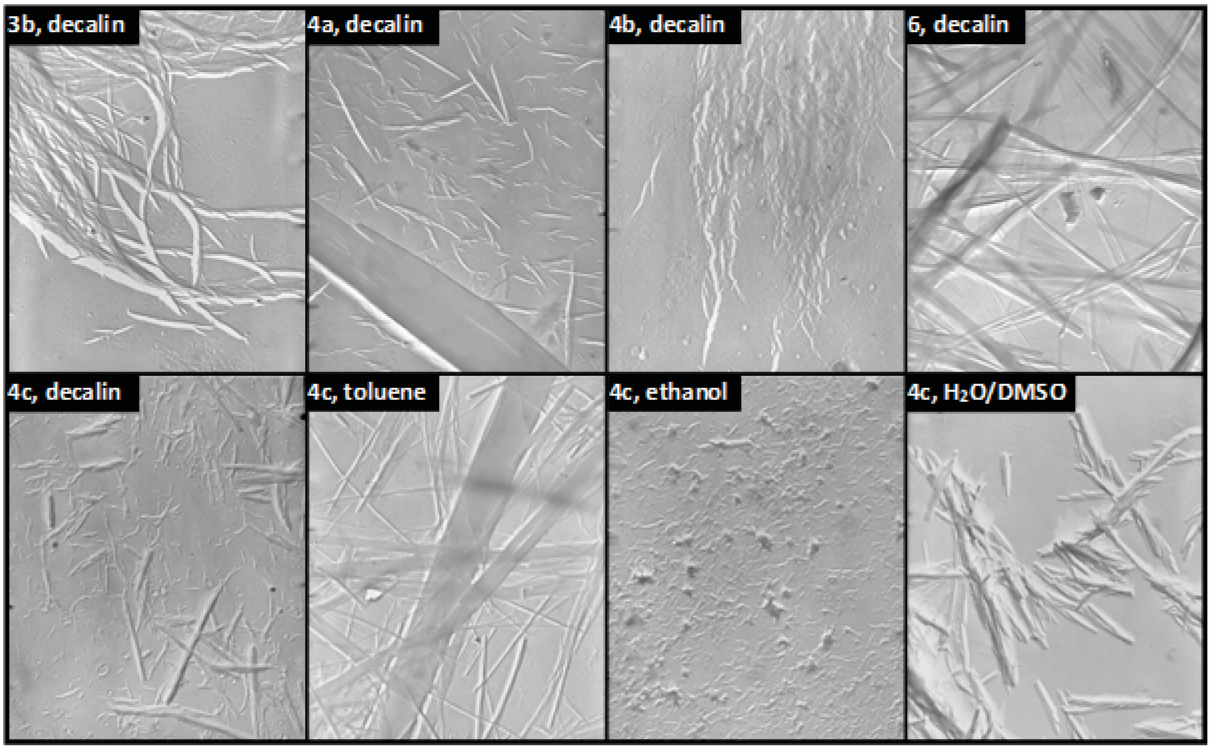


Figure 1. TEM images of xerogels. Individual window width is approximately 1 μm.

bonding. However, no bands for non-hydrogen bound amides were evident, which may reflect more efficient gelation of decalin compared to dichloromethane. Furthermore, increasing the temperature induced the **4b** decalin gel-to-sol transition (Figure S1), and the appearance of the non-hydrogen bonded N–H at 3447 cm^{-1} as well the amide I stretching at 1681 cm^{-1}. These observations strongly support the conclusion that intermolecular hydrogen bonding by amide moieties govern the gel formation.

Variable temperature ^1H NMR measurements (Figure 3) were performed on **4b** in polar and non-polar organic solvents (i.e. acetonitrile and dichloromethane) to further identify interactions governing association of molecules in solution. In both solvents, alanine amide protons are found around 7.2 ppm, indicating hydrogen bonding which weakens upon temperature increase, as judged by negative temperature coefficients of the amides. It is interesting to note that even at increased

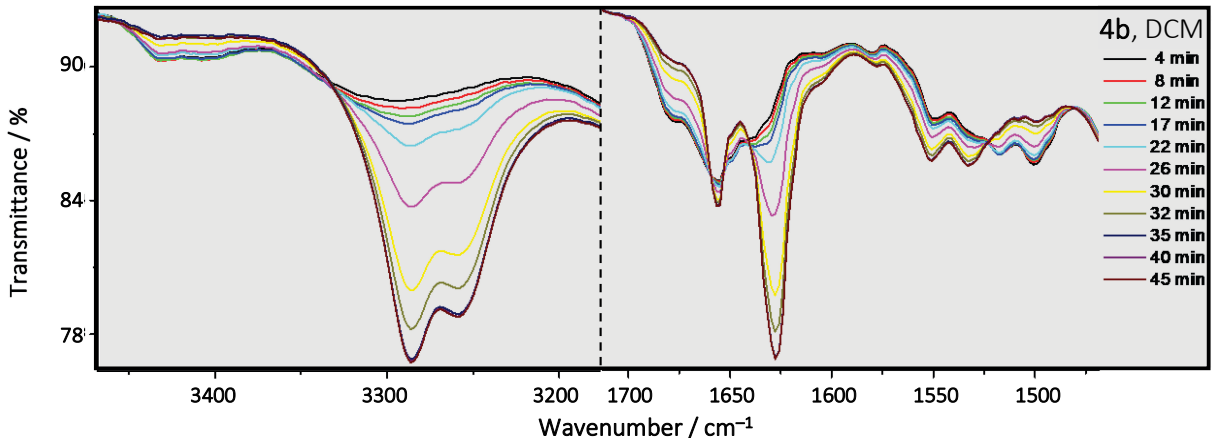


Figure 2. Time dependent FTIR spectra for **4b** dichloromethane sol-to-gel transition.

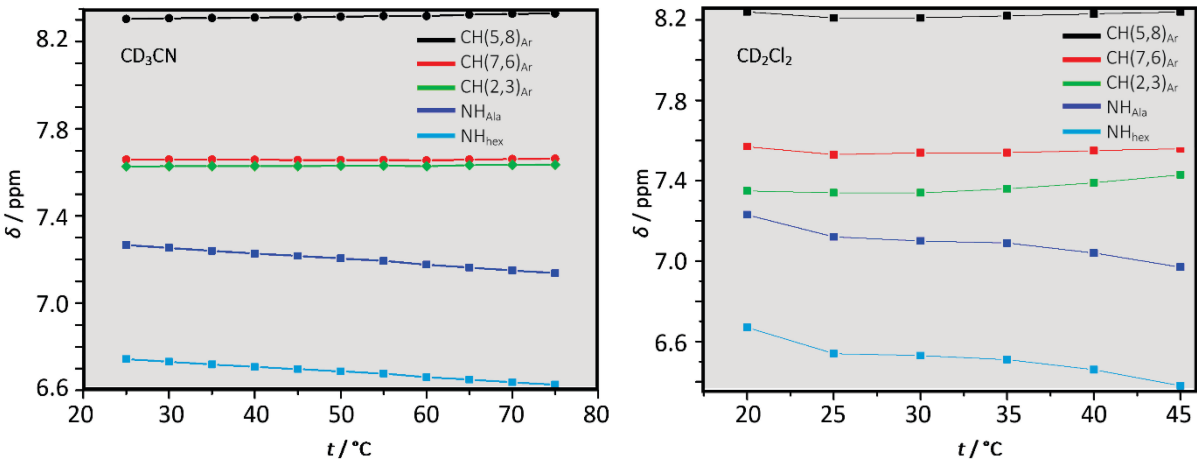


Figure 3. Chemical shifts of chosen protons from variable temperature ^{1}H NMR measurements of **4b** solution in CD_3CN (10 mM) and gel of CD_2Cl_2 (15 mM, T_g = 36 °C).

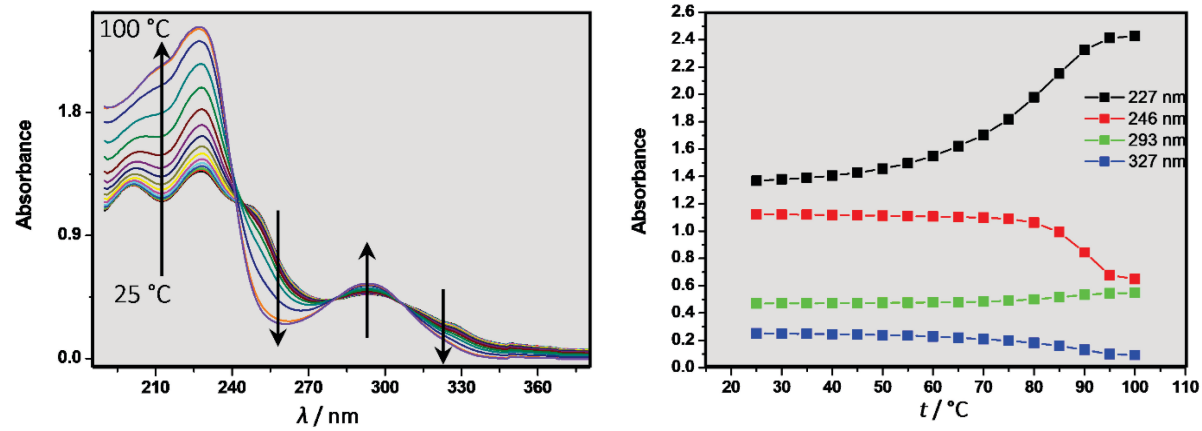


Figure 4. Variable temperature UV-Vis spectra of **6** decalin gel (82 mM).

temperatures, these protons are still above 7 ppm, indicating high propensity of the molecules for hydrogen bonding in solution. Surprisingly, variable concentration ^{1}H NMR of **4b** in CD_3CN at room temperature in the range of 0.1 to 10 mM, showed no significant changes of chemical shifts for all protons, including amides (Figure S18). This is a strong indication that the molecules in solution are substantially associated (likely dimers or small soluble oligomers) prior to gelation.

We further studied the systems using variable temperature absorption UV-Vis spectroscopy. **4b** and **4c** decalin gels exhibit absorption maxima at 292 and 298 nm, respectively (Figure S2). In the temperature range of 20 to 100 °C, only slight increase in absorption at around 230 nm was evident, indicating likely aromatic interactions within the hydrogels. Similar behaviour was observed for **3b**. On the other hand, **6** decalin gel shows substantial changes in the variable temperature UV-Vis spectra (Figure 4). The larger influence of temperature on the UV-Vis spectra changes is in qualitative agreement with the efficiency of gel formation, where stronger gelation propensity is reflected in smaller relative changes in the UV-Vis spectra.

Chiral gels were further studied by circular dichroism to investigate supramolecular chirality through aggregation of monomers. Increased ellipticity upon gel formation, from the variable temperature measurements on **4b** and **4c** decalin gels (Figure 5), strongly supports a highly ordered asymmetric organisation of molecules. The linear dichroism spectra measured at the same experimental conditions indeed confirmed negligible contribution to the circular dichroism (Figure S3). The spectra of **4b** do not change to a significant extent even up to 80 °C, indicating high stability of the aggregates, similarly observed in case of the 2,6-regioisomer **3b** (Figure S4) which is also a highly effective gelator. In contrast, for **4c** which overall exhibits lesser propensity to form gels (Table 2), the changes in the

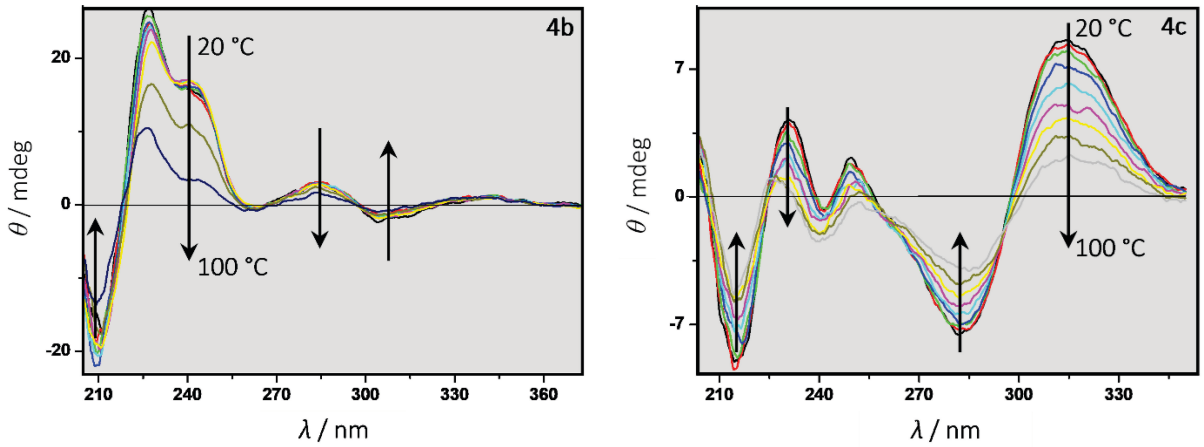


Figure 5. Temperature dependent circular dichroism spectra of decalin gels (20–100 °C, 10 °C steps) of **4b** (0.27 mM) and **4c** (1.7 mM).

spectra are gradual and significant above 40 °C. Furthermore, the observed difference between **4b** and **4c** are also in excellent agreement with the changes in UV-Vis spectra (Figure S2).

Crystal Structures

Single crystals suitable for an X-ray analysis were obtained for **1** and **5** from ethanol, polymorphs of **2** (**2m** and **2o** from ethanol and tetrahydrofurane, respectively), and **4b** from acetonitrile (Table S1). Molecular structures of these compounds are shown in Figure 6, and the numbering of atoms in Figure S42. Conformations of **1** and **5** contain an inversion centre (point group C_i). Achiral molecules of polymorphs **2m** and **2o** adopt a chiral conformation in the solid state (point group C_1); however, both conformational enantiomers are present in the crystal. **4b** is chiral due to the (*S*)-configuration of both alanine residues.

In **1** and **5**, the two substituents of the central naphthalene core are nearly coplanar (–CO–Gly–OMe in **1** and –CO–NH–C_6H_{13} in **5**). The angle between the naphthalene moiety and the directly attached amide groups is 24.77(17)° and 33.43(16)° in **1** and **5**, respectively. A notable difference in the crystal structures of **1** and **5** is evidenced by the -C1-C2-C11-O11 torsion angle: a 23.3(2)° angle in **1** cause a conformation stretched along the longer naphthalene axis, while a 144.62(14)° angle in **5** results in a conformation stretched along the shorter naphthalene axis. In the solid state, both **1** and **5** form an offset face-to-face one-dimensional tape with C11=O11···H11–N11 hydrogen bonding (Figure 7 and S44),[38] graph-set notation[39] $C(4)$, as observed for similar terephtalamide amino acid derivatives.[37,40] The significance of the N–H···O hydrogen bonds is also visible in the analysis of intermolecular contacts by calculation of

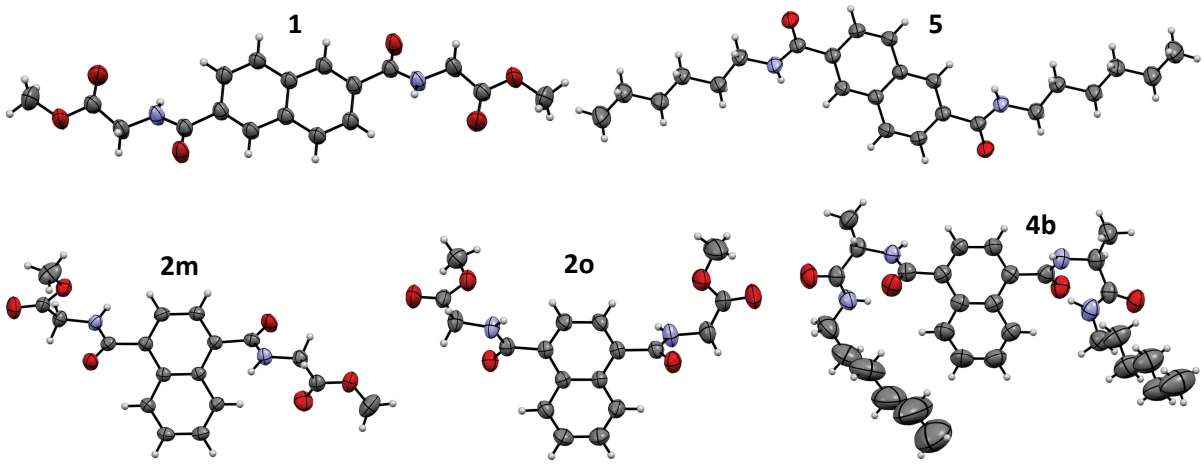


Figure 6. Molecular structures (ORTEP) of five compounds in this work. Ellipsoids are drawn at 50 % probability level.

Hirshfield surfaces[41] and fingerprint plots (Figure S43). Powder X-ray diffraction analysis (PXRD) confirmed phase purity for both **1** and **5** (Figure S45).

Two polymorphs were found for **2**. The orthorhombic polymorph, **2o** (*Pbcn*), crystallized from THF, and the phase purity of the bulk sample is confirmed by PXRD (Figure S46). Monoclinic polymorph, **2m** ($P2_1$), obtained from ethanol, revealed a mixture of the two polymorphs. Rietveld refinement was applied to estimate the **2o** to **2m** ratio as 1:3 (Figure S47). The polymorphs exhibit only minor differences in molecular conformation. For example, in **2o** the two amides form rather different angles with the central naphthalene ring (32.5(2)° and 84.7(2)°), while in **2m** these angles are similar to each other (52.8(5)° and 60.4(5)°) adopting almost an eclipsed conformation. The crystal packing of both polymorphs is dominated by *C*(4) hydrogen-bonded one-dimensional tapes, running along the *c* axis. Unlike in **1** and **5**, the neighboring hydrogen-bonded naphthalenes in the polymorphs of **2** are not parallel to each other, but form offset edge-to-face with 47.20(6)° and 68.28(11)° angles in **2o** and **2m**, respectively. A notable difference between the polymorphs of **2** is the existence π-π stacked centro-symmetric naphthalene dimers from neighboring hydrogen-bonded tapes forming 2D layers in the *bc* planes of structure **2m**. The perpendicular distance between stacked naphthalene rings is 3.4859(12) Å and the distance between their centroids is 3.8130(17) Å. Large distance of neighbouring naphthalene centroids in **2o** (> 5.6 Å) excludes the possibility of π-π stacking interactions. Therefore, in **2o**, only weak interactions between one-dimensional H-bonded chains can be found. The importance of N–H···O hydrogen bond contacts in crystal packing of **2o** and **2m** is again supported in the analysis of Hirshfield surfaces and associated fingerprint plots (Figure S43).

The most interesting crystal structure in this study was obtained for the alanine derivative **4b**. Crystals were obtained by slow crystallization of an acetonitrile gel. The crystal structure of **4b** is dominated by several N–H···O hydrogen bonds (Table S2), involving all amide bonds of the molecule. Two amide groups from the same substituent (involving N12 and N32 atoms) are connected with O21^{ii} amide oxygen atom from the molecule related by twofold screw axis with the original molecule which extrudes along *b* axis of the unit cell (Table S2). This connection is supported with additional weaker interaction C22A–H22A···O21^{ii}. Two N–H···O hydrogen bonds can be described as $R_2^1(7)$. The amide groups from the other part of molecule (those with N11 and N31 atoms) are connected with amide oxygen atoms O12^{i} and O22^{i} from the molecule related by another twofold screw axis (Table S2). This second screw axis is displaced with respect to the first one by a half period in direction of unit cell axis *a* and two hydrogen bonds involving N11 and N31 donors form a $R_2^2(12)$ motif. Therefore, a combination of these two intermolecular motifs connects molecules of **4b** in 2D layers in the *ab* planes of unit cell (Figure 7), similarly observed in other arenedicarboxamides.[42] Every molecule is surrounded with four molecules, with naphthalene cores tilted by 24.51(15)° with respect to the central one. These four molecules are also represented in the Figure S43 showing calculated Hirshfield surface of the central molecule, the corresponding fingerprint plot of intermolecular interaction, again emphasizing the importance hydrogen bonds. The layers formed are stacked one above the other only by weak van der Waals interactions between aliphatic chains of molecules.

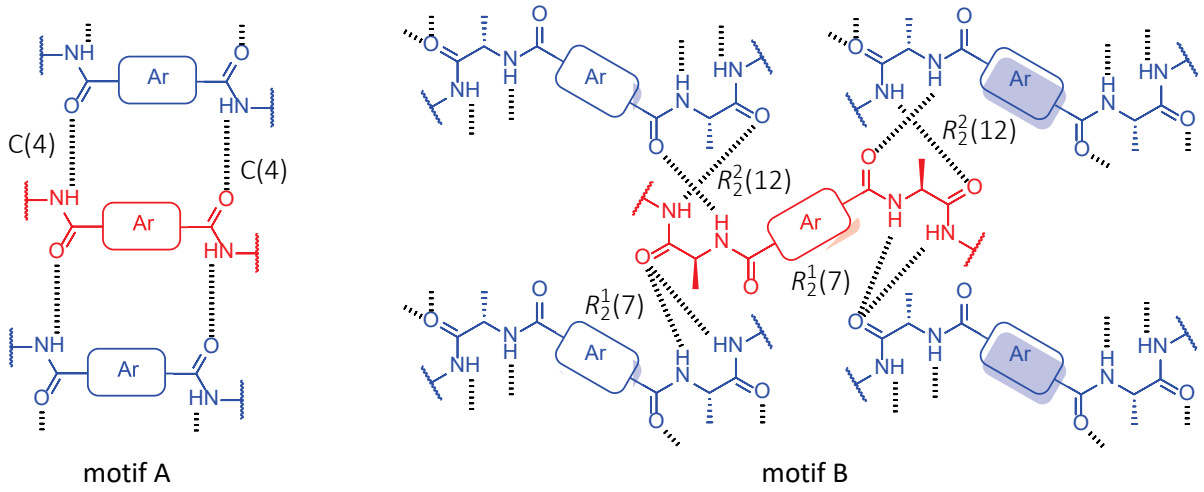


Figure 7. Different hydrogen bonding networks in the solid state: Motif A is 1D tape with two chain hydrogen-bonding pattern in **1**, **2o**, **2m** and **5**, and motif B is a 2D sheet with ring patterns in **4b**.

CONCLUSION

Herein, ten novel disubstituted naphthalene derivatives were prepared and fully characterized. We discovered that six of these compounds exhibited gelation of different organic solvents, and identified bioconjugated 1,4- and 2,6-disubstituted naphthalenes as super gelators of aromatic solvents and decalin, with critical gelling concentration well below 0.1 % *w*/*v*, reaching as low as 0.014 % for **4b**. Detailed spectroscopic (FTIR, NMR, UV-Vis) and structural (SCXRD, PXRD) investigations revealed hydrogen bonding as the main driving force for molecular association, and indicated highly stable associates in solution prior to gel formation. TEM microscopy showed different structures in the xerogels, including twisted fiber and ribbon morphologies, frequently found in different gelator systems. Our results will help establish disubstituted naphthalene bioconjugates as simple, modular, and highly efficient organogelators, and may serve as templates for supramolecular interactions in designing more elaborate supramolecular catalyst systems.

Acknowledgment. These materials are based on work financed in part by the Croatian Science Foundation (HRZZ), project numbers IP-2014-09-1461 and IP-2013-11-7387. The authors thank Ernest Sanders for technical assistance.

Supplementary Information. Supporting information to the paper is attached to the electronic version of the article at: https://doi.org/10.5562/cca4412.

PDF files with attached documents are best viewed with Adobe Acrobat Reader which is free and can be downloaded from Adobe's web site.

REFERENCES

[1] A. Hagelschuer, D. Padín, V. Dašková, B. L. Feringa, *J. Am. Chem. Soc.* **2025**, *147*, 18662–18673. https://doi.org/10.1021/jacs.5c01251

[2] Y. Sang, M. Liu, *Chem. Sci.* **2022**, *13*, 633–656. https://doi.org/10.1039/D1SC03561D

[3] M. A. Mateos-Timoneda, M. Crego-Calama, D. N. Reinhoudt, *Chem. Soc. Rev.* **2004**, *33*, 363. https://doi.org/10.1039/b305550g

[4] X. Niu, R. Zhao, S. Yan, Z. Pang, H. Li, X. Yang, K. Wang, *Small* **2023**, *19*, 2303059. https://doi.org/10.1002/smll.202303059

[5] N. M. Sangeetha, U. Maitra, *Chem. Soc. Rev.* **2005**, *34*, 821. https://doi.org/10.1039/b417081b

[6] D. K. Smith, *Soft Matter* **2024**, *20*, 10–70. https://doi.org/10.1039/D3SM01301D

[7] M. Liu, G. Ouyang, D. Niu, Y. Sang, *Org. Chem. Front.* **2018**, *5*, 2885–2900. https://doi.org/10.1039/C8QO00620B

[8] C. D. Jones, J. W. Steed, *Chem. Soc. Rev.* **2016**, *45*, 6546–6596. https://doi.org/10.1039/C6CS00435K

[9] R. Contreras-Montoya, L. Álvarez De Cienfuegos, J. A. Gavira, J. W. Steed, *Chem. Soc. Rev.* **2024**, *53*, 10604–10619. https://doi.org/10.1039/D4CS00271G

[10] E. Wang, Z. Qi, Y. Cao, R. Li, J. Wu, R. Tang, Y. Gao, R. Du, M. Liu, *Pharmaceutics* **2025**, *17*, 249. https://doi.org/10.3390/pharmaceutics17020249

[11] N. G. Serdar, T. Pospišil, M. Šišić, I. Crnolatac, P. Maleš, R. Frkanec, L. Frkanec, *Nanoscale Adv.* **2025**, *7*, 4660–4672. https://doi.org/10.1039/D5NA00033E

[12] Y. Wang, X. Sun, Q. Liu, G. Yu, *Chem. Soc. Rev.* **2025**, *54*, 3475–3512. https://doi.org/10.1039/D4CS01256A

[13] S. Zhuo, Y. Liang, Z. Wu, X. Zhao, Y. Han, B. Guo, *Mater. Horiz.* **2024**, *11*, 37–101. https://doi.org/10.1039/D3MH01403G

[14] N. Mehwish, X. Dou, Y. Zhao, C.-L. Feng, *Mater. Horiz.* **2019**, *6*, 14–44. https://doi.org/10.1039/C8MH01130C

[15] C.-W. Liu, M. Su, X.-L. Li, T. Xue, N. Liu, J. Yin, Y.-Y. Zhu, Z.-Q. Wu, *Soft Matter* **2015**, *11*, 5727–5737. https://doi.org/10.1039/C5SM00115C

[16] N. Singh, M. Kumar, J. F. Miravet, R. V. Ulijn, B. Escuder, *Chem. – Eur. J.* **2017**, *23*, 981–993. https://doi.org/10.1002/chem.201602624

[17] C. Ren, J. Zhang, M. Chen, Z. Yang, *Chem. Soc. Rev.* **2014**, *43*, 7257–7266. https://doi.org/10.1039/C4CS00161C

[18] S.-L. Yu, X.-Q. Dou, D.-H. Qu, C.-L. Feng, *J. Mol. Liq.* **2014**, *190*, 94–98. https://doi.org/10.1016/j.molliq.2013.10.031

[19] B. O. Okesola, D. K. Smith, *Chem. Soc. Rev.* **2016**, *45*, 4226–4251. https://doi.org/10.1039/C6CS00124F

[20] L. Zhang, Q. Jin, M. Liu, *Chem. – Asian J.* **2016**, *11*, 2642–2649. https://doi.org/10.1002/asia.201600441

[21] Y. Zhu, Q. Sun, Y. Lyu, J. Han, *ACS Appl. Nano Mater.* **2026**, *9*, 8478–8492. https://doi.org/10.1021/acsanm.6c00593

[22] M. Bakija, S. Opačak, B. Perić, S. Chakrabortty, A. Dell'Acqua, E. Baráth, J. G. De Vries, S. Tin, S. I. Kirin, *Dalton Trans.* **2025**, *54*, 1021–1037. https://doi.org/10.1039/D4DT02519A

[23] Z. Kokan, Z. Glasovac, M. Majerić Elenkov, M. Gredičak, I. Jerić, S. I. Kirin, *Organometallics* **2014**, *33*, 4005–4015. https://doi.org/10.1021/om5005385

[24] Z. Kokan, S. I. Kirin, *Eur. J. Org. Chem.* **2013**, *2013*, 8154–8161. https://doi.org/10.1002/ejoc.201301011

[25] J. Makarević, M. Jokić, L. Frkanec, D. Katalenić, M. Žinić, *Chem. Commun.* **2002**, *38*, 2238–2239. https://doi.org/10.1039/B206690D
[26] A. Šantić, M. Brinkkötter, T. Portada, L. Frkanec, C. Cremer, M. Schönhoff, A. Moguš-Milanković, *RSC Adv.* **2020**, *10*, 17070–17078. https://doi.org/10.1039/D0RA01249A
[27] V. Kovač, I. Kodrin, K. Radošević, K. Molčanov, B. Adhikari, H.-B. Kraatz, L. Barišić, *Organometallics* **2022**, *41*, 920–936. https://doi.org/10.1021/acs.organomet.1c00661
[28] A. Das, S. Ghosh, *Chem. Commun.* **2016**, *52*, 6860–6872. https://doi.org/10.1039/C6CC01983H
[29] A. Bera, S. K. Meena, B. Mondal, S. Roy, *Chem. – Asian J.* **2025**, *20*, e202500415. https://doi.org/10.1002/asia.202500415
[30] A. K. Rachamalla, P. K. Jana, S. Nagarajan, *Chem. – Eur. J.* **2025**, *31*, e202500001. https://doi.org/10.1002/chem.202500001
[31] N. Mehwish, X. Dou, C. Feng, *Eur. Polym. J.* **2019**, *117*, 236–253. https://doi.org/10.1016/j.eurpolymj.2019.05.034
[32] CrysAlis PRO, Agilent Technologies, Version 1.171.36.20.
[33] G. M. Sheldrick, *Acta Crystallogr., Sect. A: Found. Adv.* **2015**, *71*, 3–8. https://doi.org/10.1107/S2053273314026370
[34] G. M. Sheldrick, *Acta Crystallogr., Sect. C: Struct. Chem.* **2015**, *71*, 3–8. https://doi.org/10.1107/S2053229614024218
[35] K. Hanabusa, A. Itoh, M. Kimura, H. Shirai, *Chem. Lett.* **1999**, *28*, 767–768. https://doi.org/10.1246/cl.1999.767
[36] T. Soeta, S. Kurobe, Y. Nirei, N. Kurokawa, W. Wei, A. Yurtsever, T. Fukuma, Y. Ukaji, *Chem. – Eur. J.* **2023**, *29*, e202300455. https://doi.org/10.1002/chem.202300455
[37] B. Hachuła, A. Polasz, M. Książek, J. Kusz, V. Kozik, M. Matussek, W. Pisarski, *Tetrahedron* **2017**, *73*, 2901–2912. https://doi.org/10.1016/j.tet.2017.03.080
[38] T. Steiner, *Angew. Chem. Int. Ed.* **2002**, *41*, 48–76. https://doi.org/10.1002/1521-3773(20020104)41:1%3C48::AID-ANIE48%3E3.0.CO;2-U
[39] J. Bernstein, R. E. Davis, L. Shimoni, N. Chang, *Angew. Chem. Int. Ed. Engl.* **1995**, *34*, 1555–1573. https://doi.org/10.1002/anie.199515551
[40] A. Karmakar, C. L. Oliver, A. E. Platero-Prats, E. Laurila, L. Öhrström, *CrystEngComm* **2014**, *16*, 8243–8251. https://doi.org/10.1039/C4CE00605D
[41] P. R. Spackman, M. J. Turner, J. J. McKinnon, S. K. Wolff, D. J. Grimwood, D. Jayatilaka, M. A. Spackman, *J. Appl. Crystallogr.* **2021**, *54*, 1006–1011. https://doi.org/10.1107/S1600576721002910
[42] F. D. Lewis, J.-S. Yang, C. L. Stern, *J. Am. Chem. Soc.* **1996**, *118*, 12029–12037. https://doi.org/10.1021/ja962986b